Inorganic Chemistry Communications 180 (2025) 115044

Contents lists available at ScienceDirect

Inorganic Chemistry Communications

journal homepage: www.elsevier.com/locate/inoche

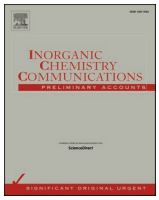

Research Article

Two-dimensional metal-organic frameworks for photocatalytic water splitting over TiO_2

Hani Nasser Abdelhamid [a,*], Haitham M. El-Bery [b]

[a] Department of Chemistry, College of Science, Imam Mohammad Ibn Saud Islamic University (IMSIU), Riyadh 11623, Saudi Arabia
[b] Department of Chemistry, Faculty of Science, Assiut University, Assiut 71515, Egypt

ARTICLE INFO

Keywords:
MOFs
Copper coordination polymers
Hydrogen production
Photocatalysis

ABSTRACT

Titanium dioxide (TiO_2) nanoparticles were reported as a photocatalyst for hydrogen production via water splitting. Herein, two-dimensional (2D) copper (Cu)-terephthalate (CuTPA) metal-organic framework (MOF) and its carbonized products were used as cocatalysts to promote the photocatalytic activity of TiO_2. The materials showed great potential in low-cost and high photocatalytic performance. They offered an environmentally friendly system for hydrogen production with initial and cumulative hydrogen generation rates (HGRs) of 12.8–23.6 mmol·h^{-1}·g^{-1} and 61.5–112.9 mmol·g^{-1}, respectively. The effects of cocatalyst loading, composite, and carbonization temperature (400 °C, 600 °C, and 800 °C) were investigated. The highest initial and cumulative HGR values were observed for CuO@C obtained after carbonization at 400 °C with 3 wt% loadings, offering HGR values of 23.6 mmol·h^{-1}·g^{-1} and 112.9 mmol·g^{-1}. CuO@C enhanced the photocatalytic performance of pristine TiO_2 by 295 and 182 folds. The combination effect of CuO and carbon nanosheet is crucial for the high photocatalytic performance of the composite cocatalyst compared to the individual cocatalysts of CuO or carbon.

1. Introduction

The energy crisis has intensified due to the increasing consumption of nonrenewable sources such as fossil fuels [1–3]. Hydrogen gas is a possible alternative energy source for the future. Nonetheless, the storage and manufacturing of hydrogen present considerable economic burdens [4–7]. Using a semiconductor catalyst in photocatalysis to split water into hydrogen and oxygen shows immense potential as a practical and environmentally friendly approach to addressing the current energy problem [8–12]. Water splitting was discussed in several reviews [13–21]. Several photocatalysts have been reported for water splitting [22,23]. The homojunction of two semiconductors of photocatalysts, such as TiO_2, promotes spatial charge separation [24,25]. According to the findings of a study that investigated picosecond transient absorption-emission spectroscopy, 90 % of photoelectrons and photoholes recombine within 10 ns during photocatalysis [26]. The photocatalytic performance of TiO_2 can be enhanced using scavengers or cocatalysts [27,28]. Several noble metals were reported as cocatalysts with high efficiencies. These noble metal cocatalysts are expensive and rare; as a result, it is difficult to employ them in hydrogen generation on a large scale. Thus, high-efficiency and low-cost cocatalysts are required to improve the photocatalytic water splitting over TiO_2 semiconductors.

Metal-organic frameworks (MOFs) have advanced the field of hydrogen generation via photocatalysis [29–38] and electrolysis [39]. They offered high photocatalytic activity for renewable energy production [40,41], carbon dioxide (CO_2) conversion or reduction [42–44]. They were also used as precursors for synthesizing metal-based catalysis embedded into a carbon framework [45,46]. MOFs and their derivatives provide advantages such as a high surface area and a well-defined structure. However, some challenges are associated with using MOFs for water splitting, e.g., low chemical stability in aqueous environments, low catalytic reactivity, and high cost. As research continues, new and improved MOFs or their derivatives are likely to be developed to enhance their performance for water splitting with high efficiency [47,48].

Herein, two-dimensional (2D) MOF of copper terephthalate (CuTPA) was carbonized for the synthesis of copper oxide-loaded carbon (CuO@C). Both precursors, i.e., CuTPA or the carbonized materials, were investigated as cocatalysts for water splitting over the semiconductor photocatalyst TiO_2. The role of carbonization temperature and composite entities, such as CuO or carbon, was investigated. CuTPA and the derived materials enhanced the photocatalytic performance of

* Corresponding author.
E-mail address: hnabdelhamid@imamu.edu.sa (H.N. Abdelhamid).

https://doi.org/10.1016/j.inoche.2025.115044
Received 14 May 2025; Received in revised form 29 June 2025; Accepted 7 July 2025
Available online 9 July 2025

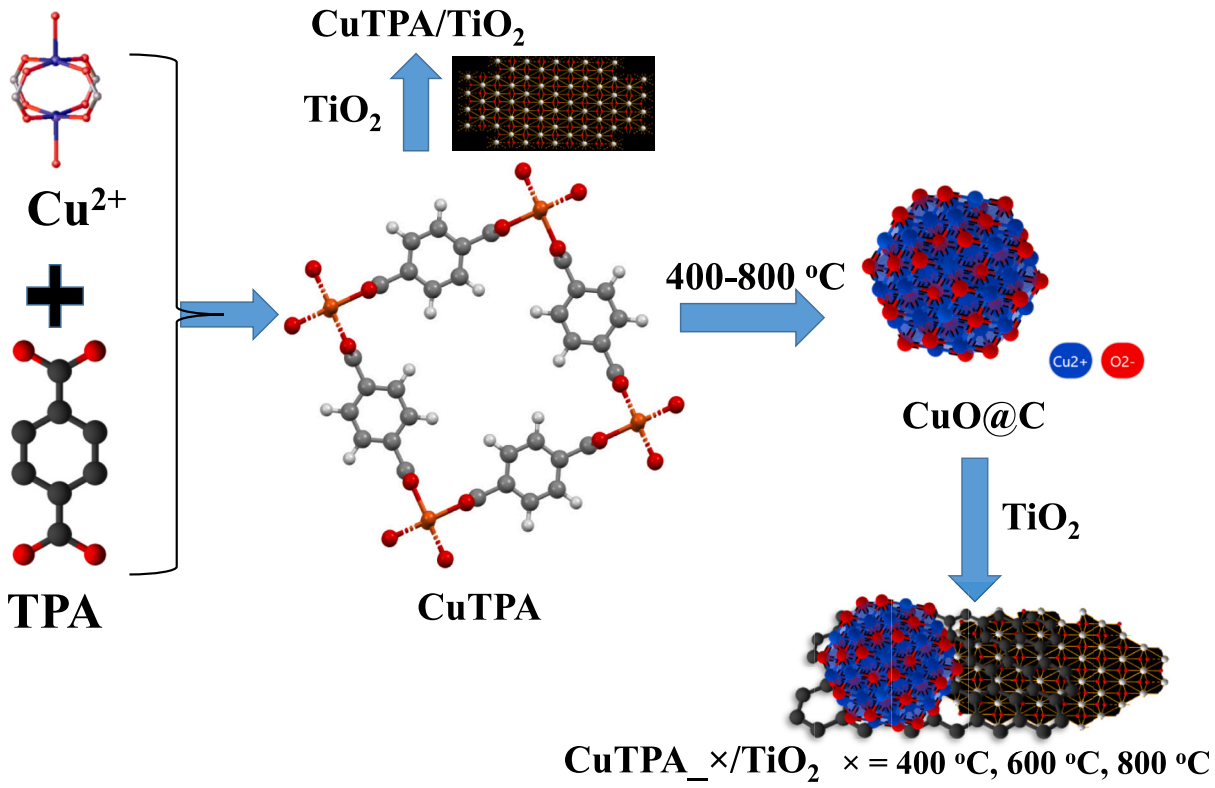

Fig. 1. Scheme for the synthesis procedure for CuTPA and its carbonization derivatives.

TiO_2, offering higher hydrogen generation rates than pristine TiO_2.

2. Experimental Section

2.1. Materials and methods

$Cu(NO_3)_2{\cdot}3H_2O$, cetrimonium bromide, and terephthalic acid (TPA) were bought from Sigma-Aldrich (Germany). Titanium dioxide photocatalyst (TiO_2, 99 %) was obtained from Aeroxide (ACROS Organics).

2.2. Synthesis of CuTPA and CuO@C

CuTPA MOF was synthesized via a solvothermal approach, as described in Reference [49]. A turquoise precipitate of CuTPA was obtained after three hours of reflux. The CuTPA MOF material was carbonized at 400–800 °C in air. The products were denoted as CuTPA_×, where × refers to the carbonized temperature, i.e., 400 °C, 600 °C, and 800 °C.

2.3. Photocatalyst preparation

$CuTPA/TiO_2$ and CuTPA_×/TiO_2 (× refers to carbonization temperatures) were synthesized using the wet impregnation technique. Typically, the cocatalysts, i.e., $CuTPA/TiO_2$ and CuTPA_×/TiO_2, were mixed in mass ratios of 0.5 %, 1 %, 2 %, 3 %, 4 %, and 5 % with TiO_2 in a ceramic evaporation dish using 0.5 mL of N-Methyl-2-pyrrolidone (NMP) and 0.5 mL of acetonitrile. The mixture was homogenized using an ultrasonic bath before solvent evaporation using a hot water bath at 80 °C. The powder was labeled as ×CuTPA/TiO_2, where × (0.5–5 %) denotes the weight fraction of CuTPA inside the composite.

A sample of carbon-loaded TiO_2 (i.e., C/TiO_2) and CuO/TiO_2 was also reported for comparison following the same procedure mentioned above. The carbon source in C/TiO_2 was obtained from carbon black (100 % compressed Thermo Scientific Chemicals). CuO was prepared via co-precipitation using a solution of NH_4OH (30 %) and calcined at 500 °C for 3 h.

2.4. Photocatalytic H_2 evolution measurements

A quartz photochemical reactor (Corrtest®, China) was used to conduct photocatalytic tests. 50 mg of photocatalyst was suspended in an aqueous methanol solution (20 wt.%), serving as a sacrificial reagent. The solution contained 200 mL of deionized water. Before the light irradiation, the photoreactor that contained the catalyst and the sacrificial reagent was swirled for approximately 30 min to allow the catalyst to spread uniformly. The photoreactor was then degassed by purging it with nitrogen gas for 30 min to eliminate any air. It was illuminated by an LED UV-light source (365 nm, 25 W, NVMUR020A, Japan). The generated hydrogen was collected at regular intervals. Hydrogen gas was analyzed using argon as the carrier gas with an inline gas chromatograph (Shimadzu GC-2014).

2.5. Characterization

X-ray diffraction (XRD) patterns were evaluated by Bruker D8 Advance, using a copper source. X-ray photoelectron spectroscopy (XPS) spectra were acquired with Al K radiation (Thermo Scientific, USA). Transmission electron microscopy (TEM) and high-resolution transmission electron microscopy (HR-TEM, JSM-2100, Japan) were employed to examine particle size, morphology, and crystal phases. Scanning transmission electron microscopy (STEM) images and energy-dispersive X-ray spectroscopy (EDX) data were collected using the same instrument. A Thermo Fisher Scientific Evolution 220 spectrophotometer (UK) was employed to obtain powdered samples' diffuse reflectance spectroscopy (DRS) spectra throughout the 200–800 nm wavelength range. Thermogravimetric analysis (TGA) curves for CuTPA and CuTPA/TiO_2 were obtained utilizing the Perkin Elmer TGA 7 apparatus.

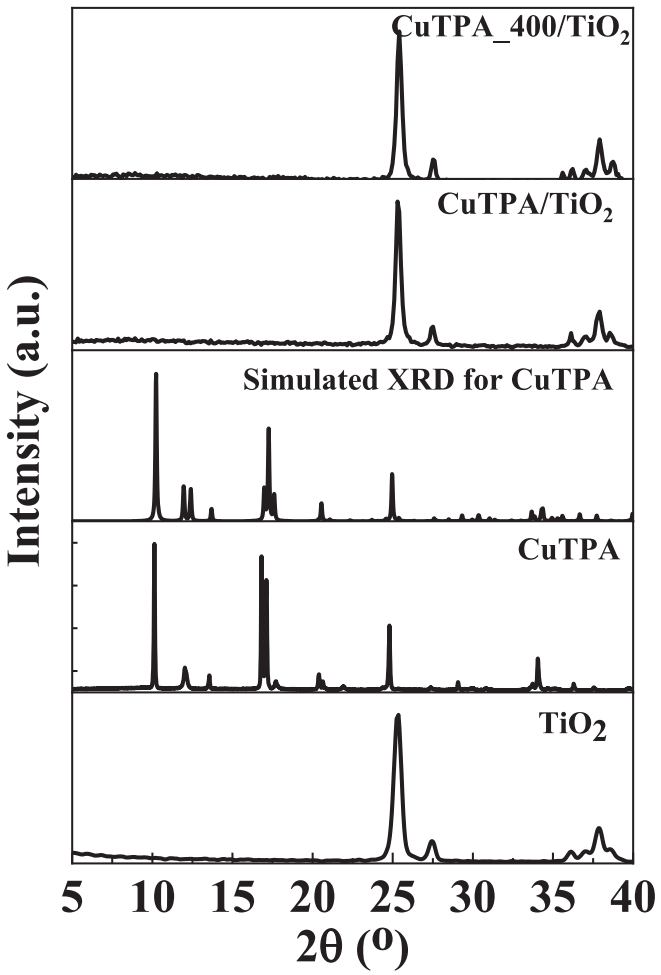

Fig. 2. XPD patterns for prepared materials.

2.6. Photoelectrochemical Measurements

The electrochemical measurements, such as cyclic voltammetry (CV), chronoamperometry (CA), and electrochemical impedance spectroscopy (EIS), were recorded using a potentiostat workstation (CS350, CorrTest® Instruments, China) in the presence of a light source consisting of UV–LED. The photocatalyst-loaded fluorine-doped tin oxide (FTO) glasses were used as a working electrode using the electrophoretic deposition method (EPD). The electrolyte solution was 0.1 M Na_2SO_4 (40 mL). The measurements were performed using a three-electrode system, with a reference electrode made out of Ag/AgCl, a counter electrode made out of Pt wire, and a working electrode made out of photocatalyst-loaded FTO substrates. EIS data were collected under dark and light irradiation, using a frequency range of 0.01–10^5 Hz.

Recyclability is a crucial aspect in assessing the long-term stability. The recyclability was evaluated according to a previous procedure using a 3CuO@C_400/TiO_2 composite, which underwent testing throughout four cycles for 20 h. For each cycle, the photocatalyst was separated via vacuum filtration using a 0.45-μm sterilized cellulose nitrate filter (Sartorius Stedium Biotech GmbH, Germany), dried at 80 °C for 12 h before the next cycle. Each run requires a freshly made aqueous methanol (20 vol%) solution. Efficiency (%) was calculated based on the ratio of HGR after 5 h for each run divided by the HGR value of the first run.

3. Results and discussion

3.1. Materials Characterization

Fig. 1 shows the synthesis of copper terephthalate (CuTPA) and CuO@C via the solvothermal method and carbonization, respectively. CuTPA was carbonized at different temperatures of 400–800 °C (Fig. 1). XRD patterns for precursor materials, i.e., TiO_2 and CuTPA, were recorded, as shown in Fig. 2. Data analysis of the XRD pattern of TiO_2 reveals the presence of a mixed phase of two TiO_2 phases, e.g., rutile and anatase crystal phases, according to the XRD simulated patterns of the JCPDS file no. 21–1272 and JCPDS file no. 21–1276 for anatase and rutile phases, respectively. The composite of CuTPA/TiO_2 and the material after carbonization at 400 °C displays mainly the diffraction pattern of TiO_2. Based on the TGA curve (**Fig. S1**), CuTPA can be decomposed starting from a temperature of 400 °C. Thus, we carbonized the materials at 400 °C, 600 °C, and 800 °C. XRD pattern of the carbonized material displays a pure phase of CuO@C with lattice parameters of a, b, c, α, β, and γ equal to 4.25 Å, 4.06 Å, 5.16 Å, 90.0°, 92.5°, and 90.0° °, respectively (**Fig. S2**).

TEM images of CuTPA (Fig. 3a) confirm the 2D morphology obtained from the crystal structure of the materials (Fig. 1). The material, e.g., CuTPA, after carbonization, displays dark particles of CuO dense phase embedded into a gray layer of carbon (Fig. 3b). TiO_2 nanoparticles were integrated into CuTPA crystal (Fig. 3c-d). CuTPA_400/TiO_2 displays two different phases of TiO_2 and CuO with gray particles referred to as carbon (Fig. 3e-f). HR-TEM images show back and white lattice fringes with a spacing distance of 0.36 nm assigned to the Miller plane (101) of TiO_2 anatase (Fig. 3e-f).

Particle morphology and elemental distribution were further characterized using STEM images (Fig. 4), EDX analysis (**Fig. S3**), and mapping (Fig. 4). STEM image of CuTPA/TiO_2 displays a big crystal of CuTPA integrated with small particles of TiO_2 nanoparticles (Fig. 4). Based on the elemental mapping of titanium, TiO_2 is homogenously distributed surrounding and on the crystal of CuTPA before and after carbonization. CuTPA and CuTPA_400 were observed surrounded by tiny crystals of TiO_2 nanoparticles (Fig. 4).

XPS analysis was included to characterize the material's elemental composition, oxidation state, and local structure (Fig. 5). The elemental survey reveals the presence of elements, specifically C 1 s, O 1 s, Ti 2p, and Cu 2p, indicating the integration of the two materials, TiO_2 and CuTPA or CuTPA_400 (Fig. 5a). The copper XPS curve displays peaks at 932.4 eV and 951.8 eV for Cu 2p3/2 and Cu 2p1/2, respectively (Fig. 5b). The titanium (Ti 2p) XPS curve shows peaks at binding energies of 458.7 eV and 464.6 eV, corresponding to Ti $2p_{3/2}$ and Ti $2p_{1/2}$, respectively (Fig. 5c).

3.2. Hydrogen Generation via Photocatalysis

The photocatalytic activities of pure TiO_2 semiconductor and its composites with CuTPA and CuTPA-carbonized at different temperatures (400–800 °C) were investigated. The role of the photocatalyst composites is investigated using cocatalysts consisting of pure carbon and CuO (**Fig. 6a**). The hydrogen generated over time for the pristine photocatalyst TiO_2 with and without the cocatalysts was recorded in **Fig. 6a**. There is a linear increase in the hydrogen generated rate (HGR) over time (**Fig. 6a**). A comparison between the different photocatalysts in terms of initial and cumulative HGR was plotted in **Fig. 6b**. TiO_2 showed initial and cumulative HGR of 0.08 and 0.62 mmol·g^{-1}, respectively (**Fig. 6b**). The low performance of pure TiO_2 can be improved by adding cocatalysts of carbon, CuO, and CuO@C obtained via the carbonization of CuTPA at 400 °C. Carbon cocatalyst enhanced the initial and cumulative HGR of TiO_2, offering values of 2.58 and 10.7 mmol·g^{-1} (**Fig. 6b**). CuO/TiO_2 offered HGR values of 12.7 and 56.8 mmol·g^{-1} (**Fig. 6b**). The highest initial and cumulative HGR values were observed for CuO@C with a 3 wt% loading, offering HGR values of 23.6

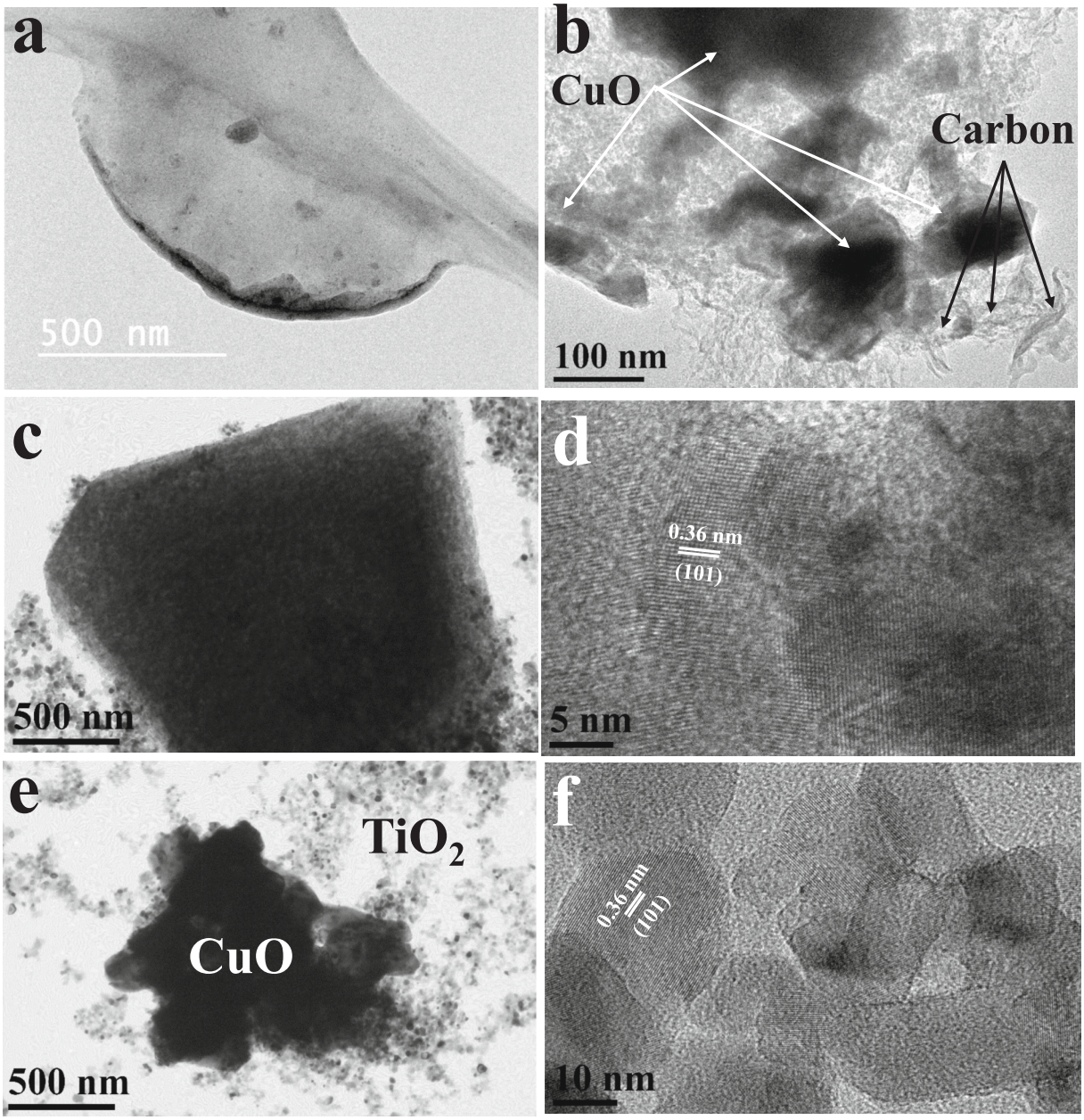

Fig. 3. TEM and HR-TEM images for a) CuTPA, b) CuTPA_400, c-d) CuTPA/TiO_2, and e-f) CuTPA_400/TiO_2.

and 112.9 mmol·g^{-1} (Fig. 6**b**). CuO@C enhanced the photocatalytic performance of pristine TiO_2 by 295 and 182 folds. The high values of HGR using CuO@C are mainly due to the synergistic effect of carbon and CuO present in CuO@C.

The effect of the CuO@C cocatalyst loading using a range of 0.5–5 wt % was investigated over time, as shown in Fig. 6**c**. Both initial and cumulative HGR values increased with the loading of CuO@C, reaching maximum values at a loading of 3 wt%. At higher loading of CuO@C (4–5 wt%), there is a decrease in the recorded HGR values (Fig. 6**d**). CuO@C/TiO_2 showed HGR values of 5.6, 15.8, 16.4, 23.6, 10.5, and 5.7 mmol·g^{-1}·h^{-1} with loading percentages of 0.5, 1, 2, 4, and 5 wt%, respectively. The drop in the photocatalytic performance of TiO_2 at higher loading of CuO@C cocatalyst could be due to the scattering of light, which prevents the interaction with the TiO_2 surface.

The effect of the carbonization temperature was also investigated using temperatures of 400 °C, 600 °C, and 800 °C. The material's initial and cumulative HGR values at the different carbonization temperatures were plotted in Fig. 7a. Cocatalyst CuTPA carbonized at 400 °C, 600 °C, and 800 °C showed initial HGR values of 23.6, 14.6, and 12.9 mmol·g^{-1}·h^{-1}, and cumulative HGR values of 112.8, 67.8, and 61.5 mmol·g^{-1}·h^{-1}, respectively (Fig. 7b). Carbonization of CuTPA above a temperature of 400 °C displays the complete decomposition of the framework into CuO with carbon residual. At high carbonization temperatures, the carbon residual decreased, and the degree of graphitization increased. Thus, the cocatalyst at high carbonization temperature showed a decrease in the recorded HGR values (Fig. 7b). The optimal carbonization temperature of CuTPA was 400 °C.

Recyclability and stability for long-time (20*h*) measurements (4 runs, 5 h for each run) were performed (Fig. 7c-d). The photocatalytic hydrogen generation can be recycled 4 times with insignificant decrease in the HGR value (Fig. 7c). HGR (mmol·g^{-1}) values and efficiency (%) are calculated for each run (after 5 h). Based on Fig. 7d, the HGR value or efficiency maintains high values after running for 20 h, indicating high recyclability and long-time efficiency. The slight decrease in HGR (112.9 mmol·g^{-1} for 1st run to 84 mmol·g^{-1} for 4th run) or efficiency (from 100 % for 1st run to 74.4 % for 4th) could be due to slight mass loss

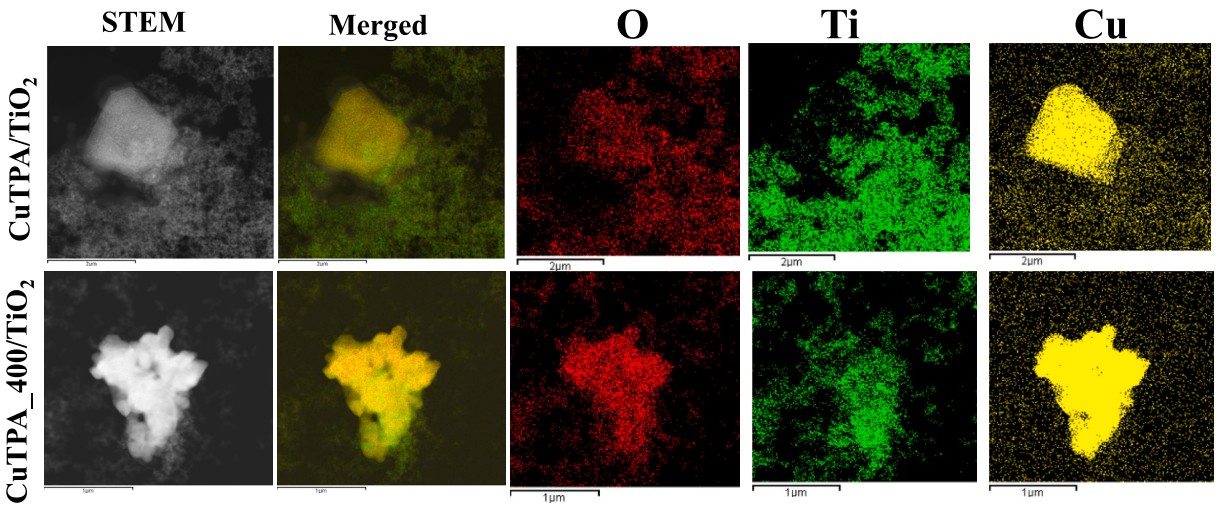

Fig. 4. STEM image and EDX elemental mapping for CuTPA/TiO_2 and CuTPA_400/TiO_2.

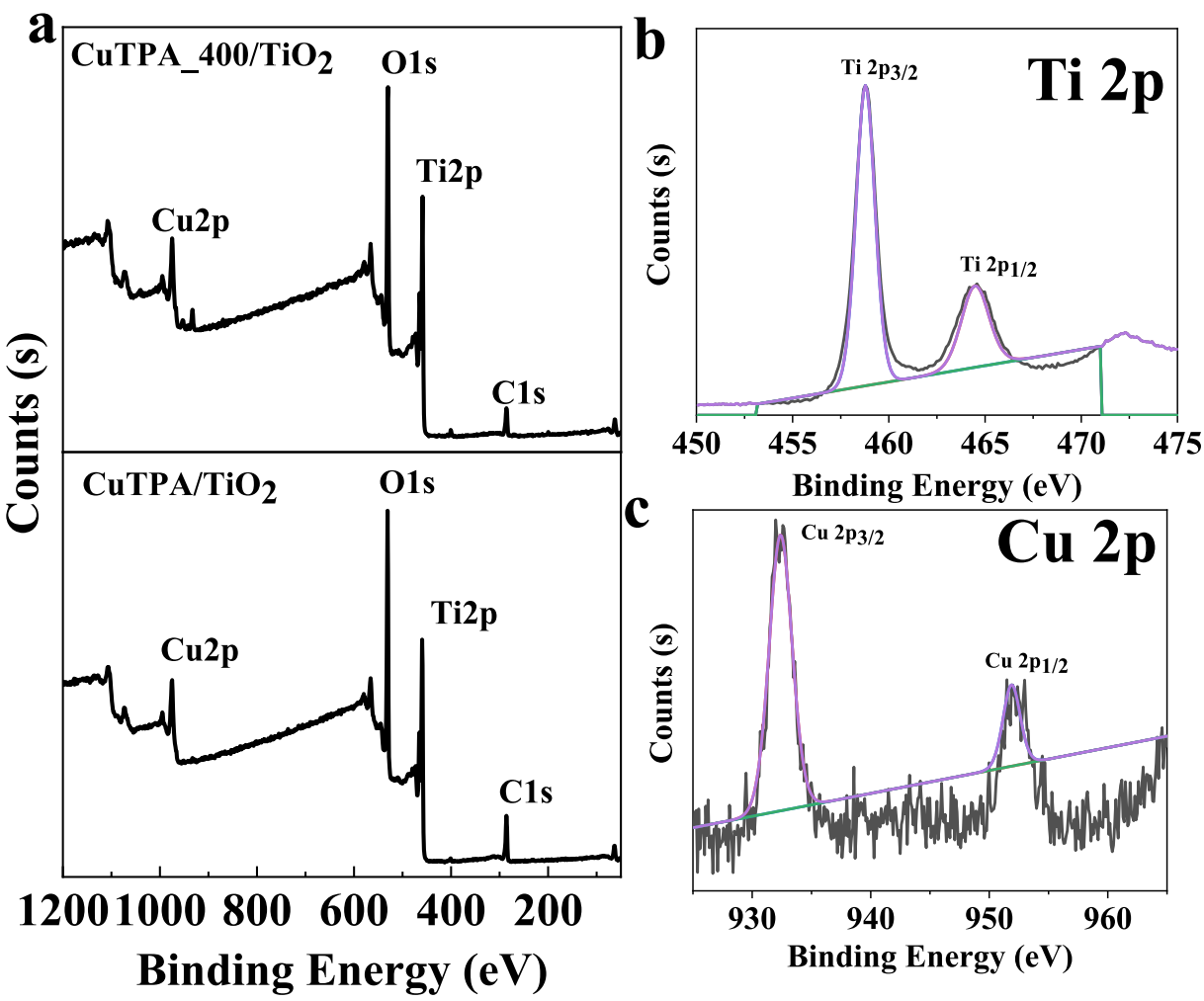

Fig. 5. XPS analysis for CuTPA/TiO_2 and CuTPA_400/TiO_2, a) survey, b) Cu 2p, and c) Ti 2p.

in photocatalysts during separation.

3.3. Mechanism of photocatalysis

The oxidation potential of the valence band (VB) of TiO_2 surpasses that of water (1.23 V vs. standard hydrogen electrode [NHE]). In comparison, the reduction potential of the conduction band (CB) of TiO_2 is less negative than the threshold for hydrogen evolution (0.00 V vs. NHE), rendering it inefficient for proton reduction to hydrogen. The valence band of TiO_2 is situated at a greater oxidation potential than that

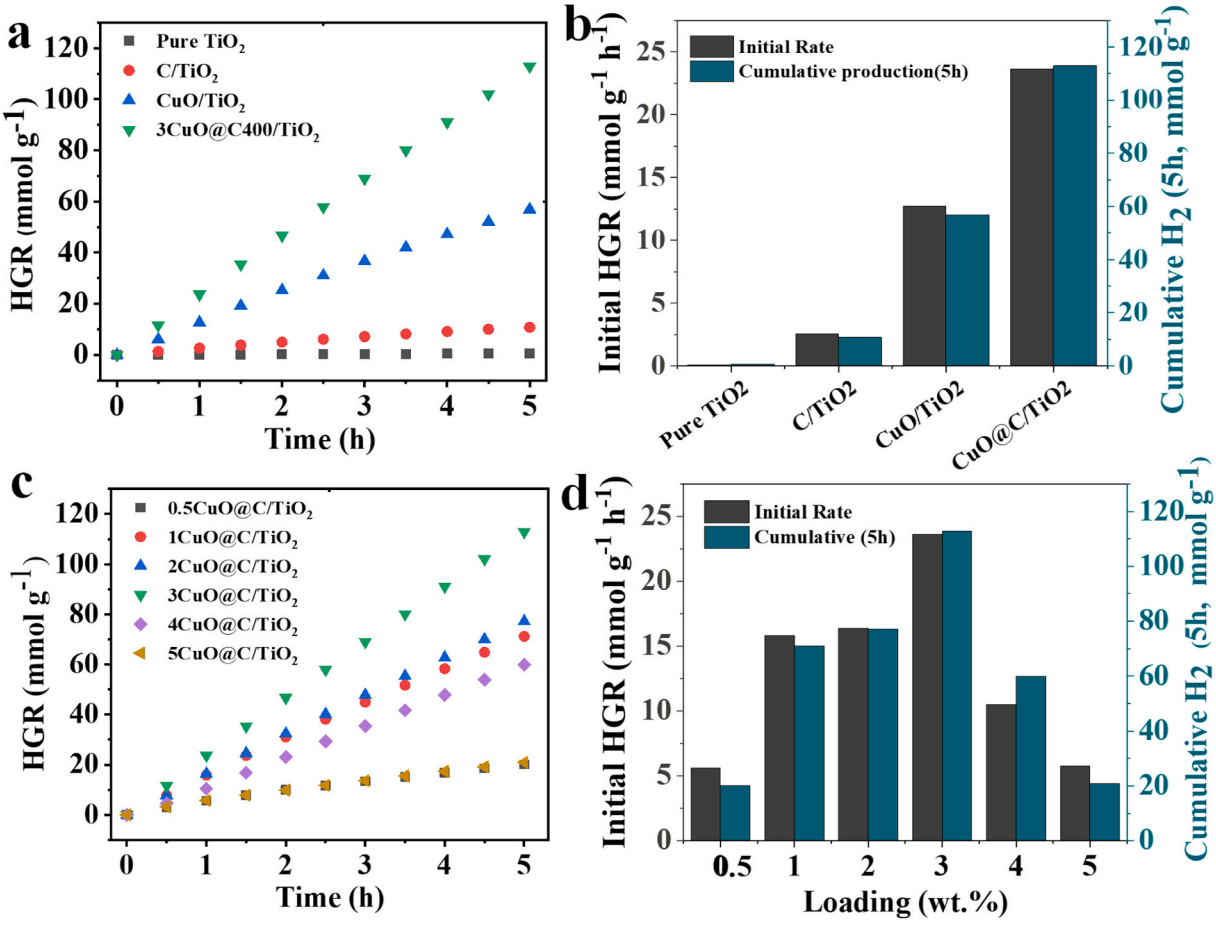

Fig. 6. a-c) HGR over time and b-d) initial and cumulative HGR for photocatalysts.

of water. The photocatalytic water splitting process consists of three essential steps: (1) light absorption and the generation of electron-hole pairs by the semiconductor TiO_2, (2) charge separation and transfer to the semiconductor surface, and (3) surface reactions resulting in the production of hydrogen and oxygen. Various data were acquired, including DRS spectra (Fig. 8**a-d**), CV (Fig. 9**a**), chronoamperometry (Fig. 9**b**), and Nyquist plots (Fig. 10a-b), to clarify the improvement noted in the photocatalytic efficacy of TiO_2.

DRS spectra of TiO_2 with and without cocatalysts were recorded, as shown in Fig. 8. The spectra for cocatalysts such as CuO and CuO@C_400 were also recorded (Fig. 8**a**). It was observed that the Degussa P25 TiO_2 exhibited a significant absorption at wavelengths of about 310 nm. Cocatalysts such as CuO@C_400 showed broad absorbance compared to CuO without carbon. All catalysts containing TiO_2 display a similar profile of pure TiO_2 photocatalyst with minimal shift due to cocatalysts with different compositions (Fig. 8**a**), carbonization temperature (Fig. 8**b-c**), and loading percentages (Fig. 8**d**). Based on Tauc plots (Fig. 8**c**), there is a shift in the optical band gap of TiO_2 (3.2 eV) to a lower value (2.9 eV) after combination with CuO@C co-catalysts. The decrease in the bandgap of pristine TiO_2 explains the higher HGR of the composite.

The electrochemical measurements of the photocatalyst with and without cocatalysts were evaluated using CV (Fig. 9**a**), chronoamperometry (Fig. 9**b**), and Nyquist plots (Fig. 10). CV data show the reduction peak of TiO_2 (Fig. 9**a**). There is an increase in the reduction current after adding CuO@C cocatalysts. The carbonized CuTPA at 400 °C exhibits the highest current values, which explains its superior photocatalytic performance compared to the other materials (Fig. 9**a**). The chronoamperometry data can also confirm these characteristics (Fig. 9**b**). Electrochemical measurements, i.e., CV and chronoamperometry, indicate that adding CuO@C enhanced the electrochemical response of TiO_2.

EIS using Nyquist plots of all photocatalysts with and without light are present in Fig. 10. A Nyquist plot is a graph of the real and imaginary parts of the impedance of a material as a function of frequency. It is a valuable tool for understanding the electrical properties of semiconductors such as TiO_2. In the case of TiO_2, the Nyquist plot typically shows a semicircle. The radius of the semicircle is related to the charge carrier mobility and the capacitance of the semiconductor. The semicircle is centered on the real axis at a value related to the semiconductor's resistance. The size and shape of the Nyquist plot can be used to assess the photoelectrochemical properties of the TiO_2 semiconductor. For example, a larger semicircle indicates higher charge carrier mobility, while a smaller semicircle indicates lower resistance. The distortion in the semicircle of TiO_2 suggests the presence of a recombination process that is undesirable for the water-splitting process. The Nyquist plot can also be used to study the effects of doping on the electrical properties of TiO_2. Adding cocatalysts, such as CuO@C and p-type materials, decreases the charge carrier concentration and mobility, which reduces the semicircle (Fig. 10). The same trend was observed without (Fig. 10a) and under light effect (Fig. 10b). Similar to data obtained from CV and chronoamperometry, Nyquist plots explain why the materials at a low carbonization temperature, i.e., 400 °C, display the highest improvement in photocatalytic activity for TiO_2.

The structure and electronic configuration of carbon alter markedly with different carbonization temperatures, affecting its physical and chemical characteristics. At low temperatures (400 °C), the produced carbon is predominantly amorphous and abundant in oxygen-containing functional groups, including hydroxyl and carboxyl, which enhance surface reactivity. As the temperature rises to the intermediate range

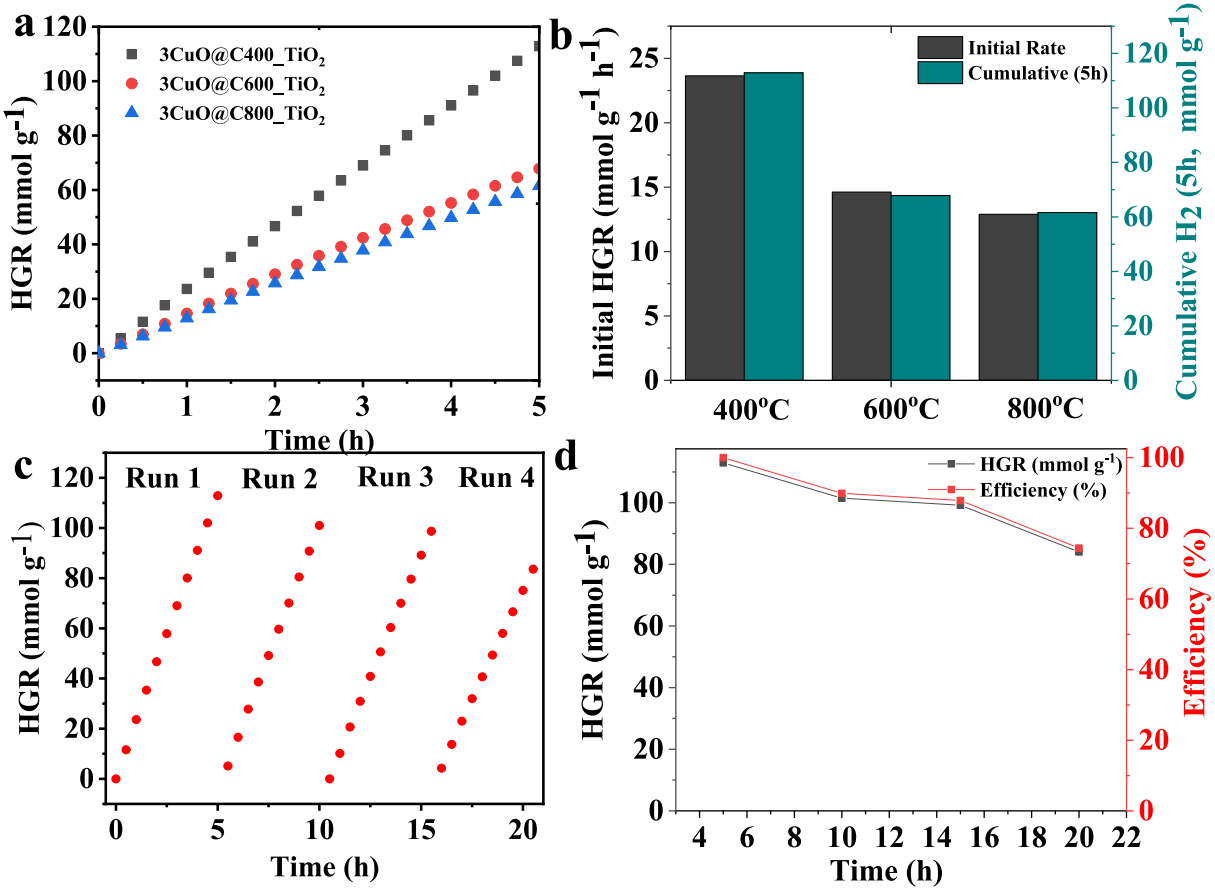

Fig. 7. Effect of carbonization temperature on hydrogen generation, a) HGR over time and b) initial and cumulative HGR for CuTPA carbonized at 400 °C, 600 °C, and 800 °C, c) recyclability, and d) HGR and efficiency for long-time measurements.

(600 °C), partial graphitization commences, resulting in improved conductivity and the formation of micropores and mesopores. The carbon exhibits increased order at high temperatures (800 °C), resulting in enhanced graphitic domain development and markedly improved conductivity. Carbonization temperature also affects the interaction forces between CuO and carbon, affecting the synergistic effect between the two materials.

Fig. 11 illustrates the basic photocatalytic process of our photocatalysts to produce hydrogen gas. In applications for the splitting of water, TiO_2, which is a kind of semiconductor with an n-type electron configuration, will function as a photoanode. When photons with an energy equal to or higher than the TiO_2 bandgap are aimed at the surface of TiO_2, the electrons in the VB will be forced to migrate into the CB, leaving holes in the VB. A p-n heterojunction was created when p-type CuO and n-type TiO_2 were brought into contact. It generated an electric field within the space charge region. Both components that went into making the composite were found to have created photoinduced holes and electrons after being exposed to light for an extended period (Fig. 11).

A comparison with other catalysts was summarized in Table 1. The synthesis procedure, such as atomic layer deposition (ALD), offered several functions, including the deposition of Cu_xO via P25 TiO_2 and the reduction of Ti^{4+} to Ti^{3+} [50]. Cu_xO/TiO_2 offered 11 times higher HGR than unmodified P25 [50]. CuO exhibits a narrow band gap; thus, it can be considered an effective candidate [51,52]. CuO can be regarded as an electron reservoir from TiO_2 [53,54]. Therefore, it prevents the recombination of electron-hole pairs, improving photocatalytic efficiency. CuO/TiO_2 was synthesized in an aqueous glycerol solution [55]. The material demonstrated effective hydrogen evolution at 2061 $\mu mol \cdot h^{-1} \cdot g^{-1}$ under UV irradiation. Nonetheless, $CuO@TiO_2$ composites synthesized via self-assembly or sol-gel techniques often encounter challenges in achieving uniform coatings with elevated specific surface areas and consistent morphologies, adversely affecting interfacial mass transfer during photocatalytic processes [55]. Conversely, heterojunctions generated through template calcination can mitigate this limitation. Cu-based catalysts are cheaper than noble metal-based photocatalysts, such as Pt-doped TiO_2 hollow spheres (Pt/HS-TiO_2) [56,57]. A cocatalyst of Cu_xO/RuO_2 improved the photocatalytic performance of $Ta_2O_5/SrZrO_3$ [58]. Cu-based TiO_2 photocatalyst exhibits high HGR values [59,60]. CuO was synthesized via hydrothermal and calcination procedures using $CuCl_2$ precursor [61]. The synthesis of CuO@C via MOF carbonization is more straightforward than most of these methods.

$[Ti_5Cu_4O_6(ba)_{16}].2CH_3CN$ (Hba = benzoic acid) was utilized to produce Cu/TiO_2@N-doped C by carbonization at 750 °C for 180 min under argon [62]. It was synthesized using a one-pot solvothermal reaction involving $Ti(OiPr)_4$, Hba, and CuCl, conducted in the presence of acetic acid and acetonitrile (CH_3CN) at 80 °C for a duration of 3 days. The Cu/TiO_2@N-doped C catalyst exhibited higher HGRs of 305 $\mu mol \cdot h^{-1} \cdot g^{-1}$ compared to Cu/TiO_2@N-doped C (182 $\mu mol \cdot h^{-1} \cdot g^{-1}$), Cu/TiO_2 (148 $\mu mol \cdot h^{-1} \cdot g^{-1}$), and TiO_2 (7 $\mu mol \cdot h^{-1} \cdot g^{-1}$), establishing the following order of average H_2 production quantum efficiency: Cu/TiO_2@N-doped C > TiO_2@N-doped C > Cu/TiO_2 > TiO_2 [63]. The data analysis indicated the oxidation of Cu during photocatalysis. A bimetallic MOF, NH_2-MIL-125(Ti/Cu), was a precursor for synthesizing $TiO_2/Cu_xO/C$ composite through carbonization at 700 °C [64]. A p (TiO_2)–n (Cu_xO) heterojunction was synthesized, providing a photocatalytic material for photocatalysis. The $TiO_2/Cu_xO/C$ nanocomposite exhibited an HGR of 3298 $\mu mol \cdot h^{-1} \cdot g^{-1}$ under UV–visible light, representing a 40-fold enhancement compared to commercial TiO_2. NH_2-MIL-125(Ti/Cu) as a precursor for synthesizing $TiO_2/Cu_xO/C$ by carbonization in an Ar/

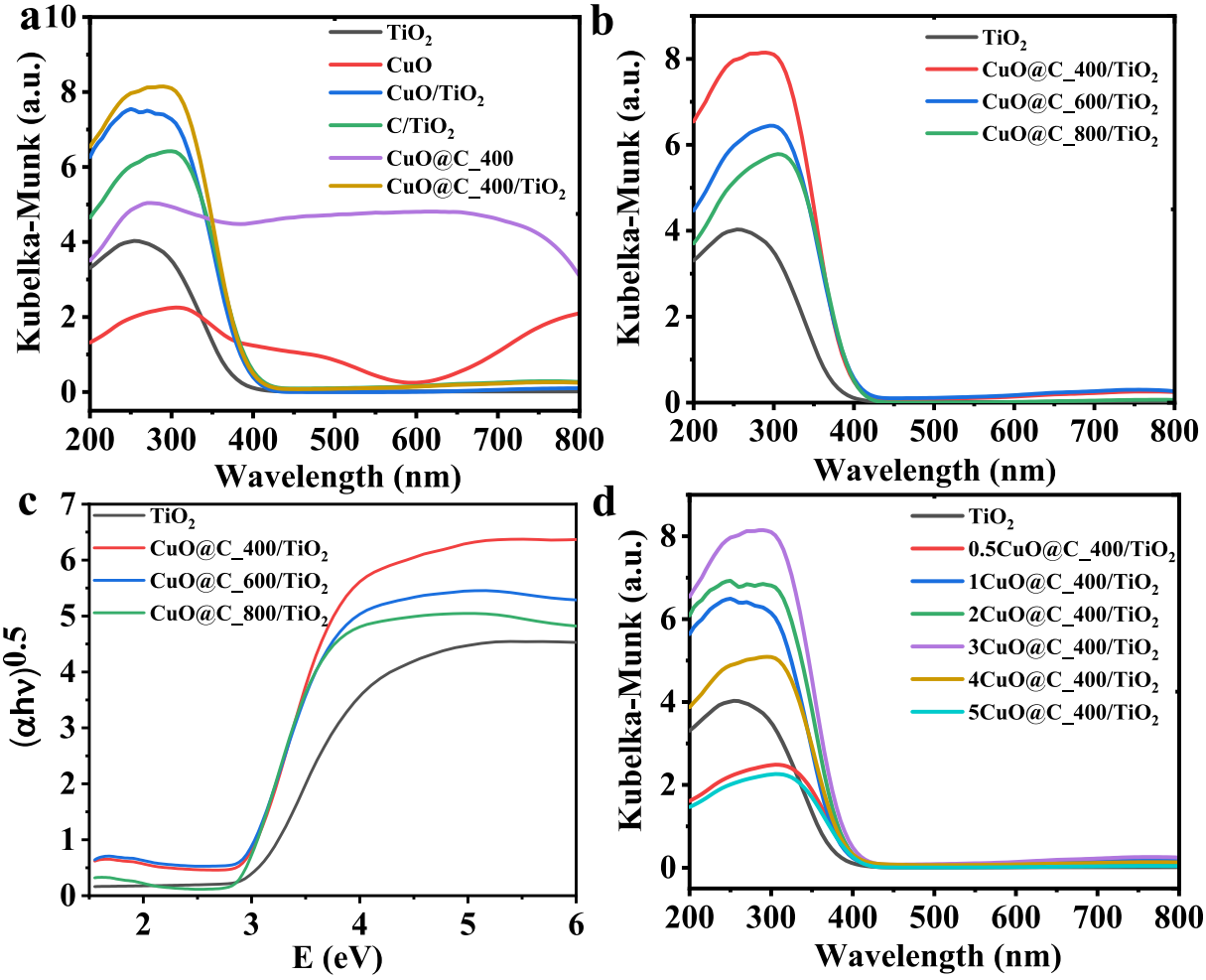

Fig. 8. a-d) UV–Vis diffuse reflectance and c) Tauc's plot.

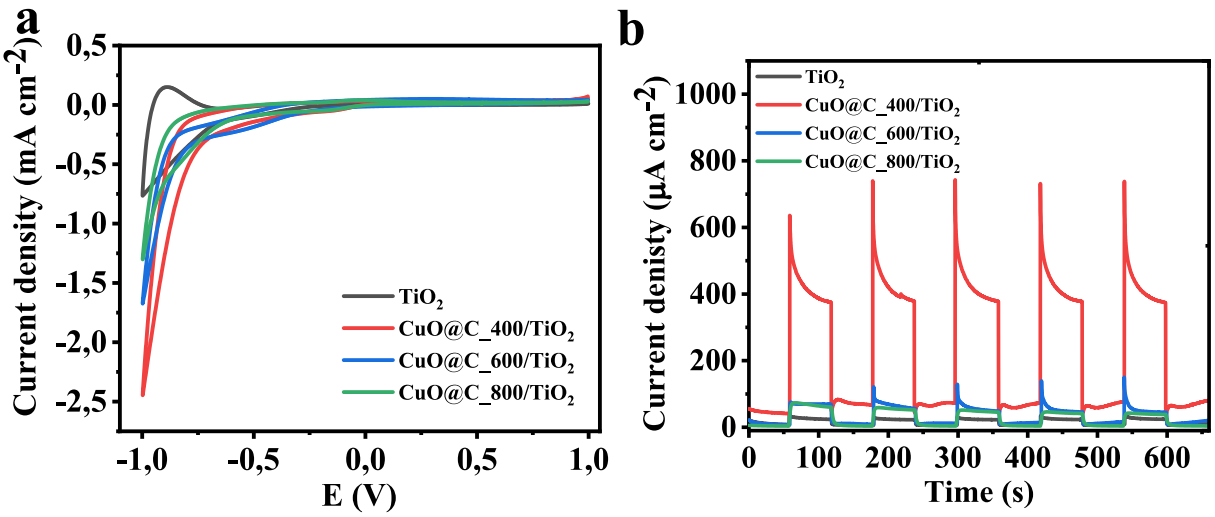

Fig. 9. a) cyclic voltammetry, and b) chronoamperometry for TiO_2 and CuTPA carbonized at different temperatures.

H_2O vapor environment. The $TiO_2/Cu_xO/C$ nanocomposite offers readily available active sites, demonstrating a remarkable photocatalytic H_2 evolution activity of 3147 $\mu mol \cdot h^{-1} \cdot g^{-1}$, which is 99 times greater than that of bare TiO_2 with only 3 wt% loading; additionally, CuO@C improves the photocatalytic activity of TiO_2 by 295 times [64].

Compared to other synthesis routes, such as ALD, solvothermal processing, or multi-step impregnation–calcination methods, the synthesis of CuTPA MOF-derived CuO@C approach is a straightforward, scalable, and cost-effective strategy for cocatalyst preparation (Table 1). MOF carbonization avoids the prolonged reaction times, high solvent consumption, and complex precursor requirements associated with solvothermal and ALD techniques. Additionally, it provides a uniform

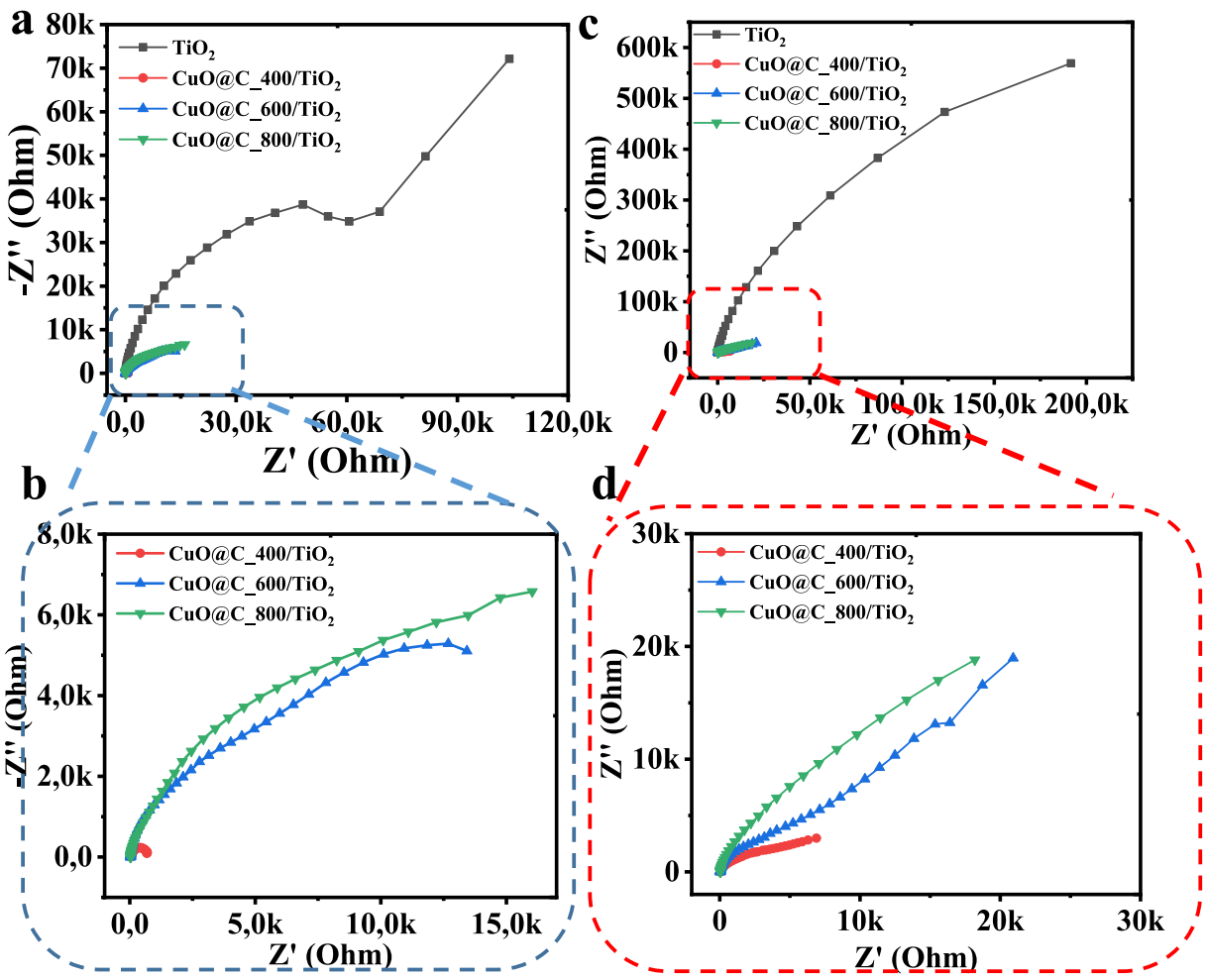

Fig. 10. Nquists plots of photocatalysts a-b) in the dark and c-d) under the light.

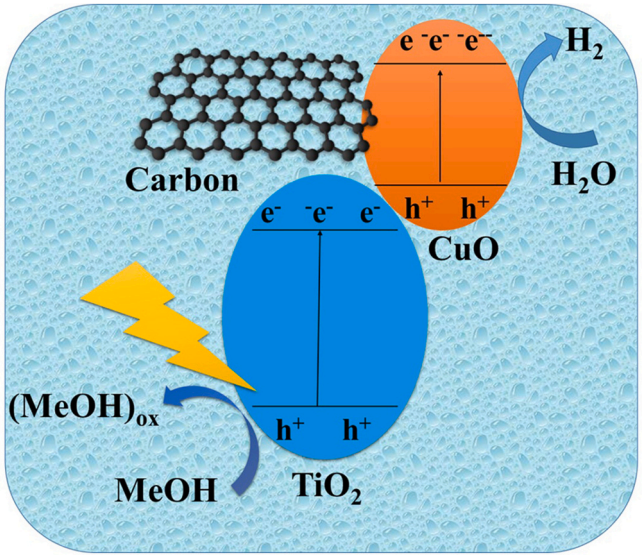

Fig. 11. Proposed mechanism for hydrogen generation via photocatalytic water splitting using CuO@/TiO_2.

distribution of Cu species within a conductive carbon matrix, facilitating charge separation and enhancing HGRs. Unlike sol-gel or self-assembly methods, which often struggle to control morphology and interfacial contact, MOF-templated calcination ensures a high surface area and a consistent nanoscale architecture (Table 1). As copper is an earth-abundant and inexpensive metal, this strategy holds significant promise for the practical, large-scale implementation of efficient TiO_2-based photocatalysts for hydrogen production.

4. Conclusions

The production of a heterojunction is a consequence of contact at the interface between the p-type semiconductor CuO@C and the n-type semiconductor TiO_2, which, in turn, causes charge to be transferred from CuO to TiO_2 and subsequently improves the separation of photo-generated electron-hole pairs and limits their recombination. The formation of the heterojunction results from the interaction of two semiconductors with separate chemical components. The difference in energy levels between two semiconductors facilitates the generation of an internal electric field, enhancing the transit and separation of charge carriers. Thus, CuO@C improved the photocatalytic performance of TiO_2 in terms of high HGRs.

CRediT authorship contribution statement

Hani Nasser Abdelhamid: Writing – review & editing, Writing – original draft, Visualization, Validation, Supervision, Software, Resources, Project administration, Methodology, Investigation, Funding acquisition, Formal analysis, Data curation, Conceptualization. **Haitham M. El-Bery:** Writing – review & editing, Resources, Methodology, Investigation, Formal analysis, Data curation.

Table 1
Summary of Copper-based cocatalyst enhanced photocatalytic performance of TiO_2.

Photocatalysts	Synthesis Procedure	Conditions	Photocatalysis condition	HGR ($mmol \cdot h^{-1} \cdot g^{-1}$)	Ref.
CuO/TiO_2	1. Hydrothermal 2. Calcination	• 200 °C for 24 h • 400 °C for 2 h in air	Cat. 20 mg, aqueous methanol solution (methanol 10 mL + distilled water 90 mL), 300 W Xe lamp	2	[61]
Cu/TiO_2@N-doped C		Heating at 750 °C under Ar for 180 min	Cat. 10 mg, aqueous solution (8 mL) containing triethanolamine (TEOA) (8 vol%), 300 W xenon lamp	0.305	[62]
$TiO_2/Cu_xO/C$	Steam Carbonization	➢ 130 °C, for 40 h ➢ 120 °C for 12 h ➢ 700 °C in water vapor for 2 h	Cat. 10 mg, 7.5 mL of CH_3OH and 17.5 mL of H_2O, 500 W Xe/Hg lamp	3.298	[65]
$TiO_2/Cu_xO/C$	1. Impregnation 2. Carbonization	➢ 130 °C for 40 h ➢ Impregnation heating at 110 °C for 12 h ➢ 700 °C for 2 h	Cat. 10 mg, deionized water (17.5 mL), and methanol (7.5 mL), 500 W Xe/Hg lamp	3.147	[64]
$TiO_2/CuO/C$	1. Carbonization 2. Impregnation	➢ 400 °C for 2 h ➢ 100 °C for 30 min	Cat. 50 mg, deionized water and methanol, 25 W LED lamp	12.8–23.6	Here

Funding

This work was supported and funded by the Deanship of Scientific Research at Imam Mohammad Ibn Saud Islamic University (IMSIU) (grant number IMSIU-DDRSP2503).

Declaration of competing interest

The authors declare that they have no known competing financial interests or personal relationships that could have appeared to influence the work reported in this paper.

Appendix A. Supplementary data

Supplementary data to this article can be found online at https://doi.org/10.1016/j.inoche.2025.115044.

Data availability

Data will be made available on request.

References

[1] S. Yaghoubi, S.M. Mousavi, A. Babapoor, M. Binazadeh, C.W. Lai, R.H. Althomali, M.M. Rahman, W.-H. Chiang, Photocatalysts for solar energy conversion: recent advances and environmental applications, Renew. Sust. Energ. Rev. 200 (2024) 114538, https://doi.org/10.1016/j.rser.2024.114538.
[2] H. Cai, P. Zhang, B. Li, Y. Zhu, Z. Zhang, W. Guo, High-entropy oxides for energy-related electrocatalysis, Mater. Today Catal. 4 (2024) 100039, https://doi.org/10.1016/j.mtcata.2024.100039.
[3] R. Deng, M. Gao, B. Zhang, Q. Zhang, Solvent-mediated synthesis of functional powder materials from deep eutectic solvents for energy storage and conversion: a review, Adv. Energy Mater. 14 (2024), https://doi.org/10.1002/aenm.202303707.
[4] D. Wei, X. Shi, R. Qu, K. Junge, H. Junge, M. Beller, Toward a hydrogen economy: development of heterogeneous catalysts for chemical hydrogen storage and release reactions, ACS Energy Lett. 7 (2022) 3734–3752, https://doi.org/10.1021/acsenergylett.2c01850.
[5] H.N. Abdelhamid, A review on hydrogen generation from the hydrolysis of sodium borohydride, Int. J. Hydrog. Energy 46 (2021) 726–765, https://doi.org/10.1016/j.ijhydene.2020.09.186.
[6] H.N. Abdelhamid, Ti3AlC2 MAX/MXene for hydrogen generation via photocatalytic hydride hydrolysis, Inorganics 13 (2025) 44, https://doi.org/10.3390/inorganics13020044.
[7] S. Onajah, R. Sarkar, M.S. Islam, M. Lalley, K. Khan, M. Demir, H.N. Abdelhamid, A.A. Farghaly, Silica-derived nanostructured electrode materials for ORR, OER, HER, CO_2 RR Electrocatalysis, and energy storage applications: a review, Chem. Rec. 24 (2024) e202300234, https://doi.org/10.1002/tcr.202300234.
[8] K. Wenderich, G. Mul, Methods, mechanism, and applications of Photodeposition in Photocatalysis: a review, Chem. Rev. 116 (2016) 14587–14619, https://doi.org/10.1021/acs.chemrev.6b00327.
[9] W.S. Koe, J.W. Lee, W.C. Chong, Y.L. Pang, L.C. Sim, An overview of photocatalytic degradation: photocatalysts, mechanisms, and development of photocatalytic membrane, Environ. Sci. Pollut. Res. 27 (2020) 2522–2565, https://doi.org/10.1007/s11356-019-07193-5.
[10] X. Li, J. Yu, S. Wageh, A.A. Al-Ghamdi, J. Xie, Graphene in Photocatalysis: a review, Small 12 (2016) 6640–6696, https://doi.org/10.1002/smll.201600382.
[11] H. Tong, S. Ouyang, Y. Bi, N. Umezawa, M. Oshikiri, J. Ye, Nano-photocatalytic materials: possibilities and challenges, Adv. Mater. 24 (2012) 229–251, https://doi.org/10.1002/adma.201102752.
[12] D.S. Bhatkhande, V.G. Pangarkar, A.A.C.M. Beenackers, Photocatalytic degradation for environmental applications – a review, J. Chem. Technol. Biotechnol. 77 (2002) 102–116, https://doi.org/10.1002/jctb.532.
[13] M. Ashokkumar, An overview on semiconductor particulate systems for photoproduction of hydrogen, Int. J. Hydrog. Energy 23 (1998) 427–438, https://doi.org/10.1016/S0360-3199(97)00103-1.
[14] C.-H. Liao, C.-W. Huang, J.C.S. Wu, Hydrogen production from semiconductor-based Photocatalysis via water splitting, Catalysts 2 (2012) 490–516, https://doi.org/10.3390/catal2040490.
[15] M. Ni, M.K.H. Leung, D.Y.C. Leung, K. Sumathy, A review and recent developments in photocatalytic water-splitting using TiO2 for hydrogen production, Renew. Sust. Energ. Rev. 11 (2007) 401–425, https://doi.org/10.1016/j.rser.2005.01.009.
[16] A.K. Hussein, Applications of nanotechnology in renewable energies—a comprehensive overview and understanding, Renew. Sust. Energ. Rev. 42 (2015) 460–476, https://doi.org/10.1016/j.rser.2014.10.027.
[17] T. Jafari, E. Moharreri, A. Amin, R. Miao, W. Song, S. Suib, Photocatalytic water splitting—the untamed dream: a review of recent advances, Molecules 21 (2016) 900, https://doi.org/10.3390/molecules21070900.
[18] C. Acar, I. Dincer, G.F. Naterer, Review of photocatalytic water-splitting methods for sustainable hydrogen production, Int. J. Energy Res. 40 (2016) 1449–1473, https://doi.org/10.1002/er.3549.
[19] N. Fajrina, M. Tahir, A critical review in strategies to improve photocatalytic water splitting towards hydrogen production, Int. J. Hydrog. Energy 44 (2019) 540–577, https://doi.org/10.1016/j.ijhydene.2018.10.200.
[20] C.C. Nguyen, N.N. Vu, T.-O. Do, Recent advances in the development of sunlight-driven hollow structure photocatalysts and their applications, J. Mater. Chem. A 3 (2015) 18345–18359, https://doi.org/10.1039/C5TA04326C.
[21] T. Suguro, F. Kishimoto, K. Takanabe, Photocatalytic hydrogen production under water vapor feeding—a Minireview, Energy Fuel 36 (2022) 8978–8994, https://doi.org/10.1021/acs.energyfuels.2c01478.
[22] S.M. Thabet, H.N. Abdelhamid, S.A. Ibrahim, H.M. El-Bery, Boosting photocatalytic water splitting of TiO2 using metal (Ru, Co, or Ni) co-catalysts for hydrogen generation, Sci. Rep. 14 (2024) 10115, https://doi.org/10.1038/s41598-024-59608-0.
[23] M. Saleh, H.N. Abdelhamid, D.M. Fouad, H.M. El-Bery, Enhancing photocatalytic water splitting: comparative study of TiO2 decorated nanocrystals (Pt and cu) using different synthesis methods, Fuel 354 (2023) 129248, https://doi.org/10.1016/j.fuel.2023.129248.
[24] Y. Zhao, X. Huang, X. Tan, T. Yu, X. Li, L. Yang, S. Wang, Fabrication of BiOBr nanosheets@TiO2 nanobelts p–n junction photocatalysts for enhanced visible-light activity, Appl. Surf. Sci. 365 (2016) 209–217, https://doi.org/10.1016/j.apsusc.2015.12.249.
[25] J. Low, J. Yu, M. Jaroniec, S. Wageh, A.A. Al-Ghamdi, Heterojunction Photocatalysts, Adv. Mater. 29 (2017) 1601694, https://doi.org/10.1002/adma.201601694.
[26] N. Serpone, D. Lawless, R. Khairutdinov, E. Pelizzetti, Subnanosecond relaxation dynamics in TiO2 colloidal sols (particle sizes Rp = 1.0-13.4 nm). Relevance to heterogeneous Photocatalysis, J. Phys. Chem. 99 (1995) 16655–16661, https://doi.org/10.1021/j100045a027.
[27] D.W. Bahnemann, M. Hilgendorff, R. Memming, Charge carrier dynamics at TiO2 particles: reactivity of free and trapped holes, J. Phys. Chem. B 101 (1997) 4265–4275, https://doi.org/10.1021/jp9639915.
[28] R. Abe, K. Sayama, H. Arakawa, Significant effect of iodide addition on water splitting into H2 and O2 over Pt-loaded TiO2 photocatalyst: suppression of backward reaction, Chem. Phys. Lett. 371 (2003) 360–364, https://doi.org/10.1016/S0009-2614(03)00252-5.
[29] R. Pavithran, M.N.S. Sreevidya, Metal−Organic Frameworks as Photocatalysts for Hydrogen Evolution, 2021, pp. 499–511, https://doi.org/10.1021/bk-2021-1393.ch017.
[30] J. Chen, R. Abazari, K.A. Adegoke, N.W. Maxakato, O.S. Bello, M. Tahir, S. Tasleem, S. Sanati, A.M. Kirillov, Y. Zhou, Metal–organic frameworks and

derived materials as photocatalysts for water splitting and carbon dioxide reduction, Coord. Chem. Rev. 469 (2022) 214664, https://doi.org/10.1016/j.ccr.2022.214664.
[31] E. Nyela Musa, K.C. Stylianou, Metal–organic framework-derived semiconductors for photocatalytic hydrogen production, Mol. Syst. Des. Eng. (2023), https://doi.org/10.1039/D2ME00221C.
[32] Y. Shi, A.-F. Yang, C.-S. Cao, B. Zhao, Applications of MOFs: recent advances in photocatalytic hydrogen production from water, Coord. Chem. Rev. 390 (2019) 50–75, https://doi.org/10.1016/j.ccr.2019.03.012.
[33] X. Chen, X. Peng, L. Jiang, X. Yuan, H. Yu, H. Wang, J. Zhang, Q. Xia, Recent advances in titanium metal–organic frameworks and their derived materials: features, fabrication, and photocatalytic applications, Chem. Eng. J. 395 (2020) 125080, https://doi.org/10.1016/j.cej.2020.125080.
[34] J. Gao, Q. Huang, Y. Wu, Y.-Q. Lan, B. Chen, Metal–Organic Frameworks for Photo/Electrocatalysis, Adv. Energy Sustain. Res. 2 (2021) 2100033, https://doi.org/10.1002/aesr.202100033.
[35] S. Liu, C. Zhang, Y. Sun, Q. Chen, L. He, K. Zhang, J. Zhang, B. Liu, L.-F. Chen, Design of metal-organic framework-based photocatalysts for hydrogen generation, Coord. Chem. Rev. 413 (2020) 213266, https://doi.org/10.1016/j.ccr.2020.213266.
[36] X. Li, Q. Dong, Q. Tian, A. Sial, H. Wang, H. Wen, B. Pan, K. Zhang, J. Qin, C. Wang, Recent advance in metal- and covalent-organic framework-based photocatalysis for hydrogen evolution, Mater. Today Chem. 26 (2022) 101037, https://doi.org/10.1016/j.mtchem.2022.101037.
[37] A.B.A. Abdellatif, H.M. El-Bery, H.N. Abdelhamid, S.A. El-Gyar, ZIF-67 and cobalt-based@heteroatom–doped carbon nanomaterials for hydrogen production and dyes removal via adsorption and catalytic degradation, J. Environ. Chem. Eng. 10 (2022) 108848, https://doi.org/10.1016/j.jece.2022.108848.
[38] H.N. Abdelhamid, A.B.A. Abdellatif, H.M. El-Bery, Hydrogen production using noble metal-free metal-organic frameworks (MOFs)-derived CuO@C/TiO_2, Chem. Eng. J. 514 (2025) 163343, https://doi.org/10.1016/j.cej.2025.163343.
[39] A.Z. Alhakemy, M.H. Elsayed, F.K. Algethami, H.N. Abdelhamid, Metal-organic framework (MOF)-derived bimetallic (Ni, Cu) oxide@C electrocatalyst for oxygen evolution reaction, Int. J. Hydrog. Energy 115 (2025) 289–298, https://doi.org/10.1016/j.ijhydene.2025.01.206.
[40] N.A. Nordin, M.A. Mohamed, M.N.I. Salehmin, S.F., Mohd Yusoff, photocatalytic active metal–organic framework and its derivatives for solar-driven environmental remediation and renewable energy, Coord. Chem. Rev. 468 (2022) 214639, https://doi.org/10.1016/j.ccr.2022.214639.
[41] S. Guo, C. Pan, M. Hou, Y. Hou, S. Yao, T. Lu, Z. Zhang, Dual Regulation of Sensitizers and Cluster Catalysts in Metal–Organic Frameworks to Boost H_2 Evolution, Angew. Chem. Int. Ed. 64 (2025), https://doi.org/10.1002/anie.202420398.
[42] Y. Wang, X. Cheng, N. Ma, W. Cheng, P. Zhang, F. Luo, W. Shi, S. Yao, T. Lu, Z. Zhang, In situ growth of metal-organic layer on Polyoxometalate-etching Cu_2O to boost CO_2 reduction with high stability, Angew. Chem. Int. Ed. 64 (2025), https://doi.org/10.1002/anie.202423204.
[43] H.-Q. Yin, Z.-M. Zhang, T.-B. Lu, Ordered integration and Heterogenization of catalysts and photosensitizers in metal-/covalent-organic frameworks for boosting CO2 Photoreduction, Acc. Chem. Res. 56 (2023) 2676–2687, https://doi.org/10.1021/acs.accounts.3c00380.
[44] J.-W. Wang, L.-Z. Qiao, H.-D. Nie, H.-H. Huang, Y. Li, S. Yao, M. Liu, Z.-M. Zhang, Z.-H. Kang, T.-B. Lu, Facile electron delivery from graphene template to ultrathin metal-organic layers for boosting CO_2 photoreduction, Nat. Commun. 12 (2021) 813, https://doi.org/10.1038/s41467-021-21084-9.
[45] H.N. Abdelhamid, Bimetallic Metal–Organic Framework (MOF)–Derived NiO/CuO-Embedded Carbon for Supercapacitor, Appl. Organomet. Chem. 39 (2025) e70193, https://doi.org/10.1002/aoc.70193.
[46] W. Sharmoukh, Z.M. Hassan, S.G. Mohamed, H.N. Abdelhamid, Metal-organic frameworks (UiO66-NH_2)/PEDOT-derived ZrO_2/N, S-doped carbon for supercapacitors, J. Energy Storage. 102 (2024) 114071, https://doi.org/10.1016/j.est.2024.114071.
[47] H.M. El-Bery, H.N. Abdelhamid, Photocatalytic hydrogen generation via water splitting using ZIF-67 derived Co_3O_4@C/TiO_2, J. Environ. Chem. Eng. 9 (2021) 105702, https://doi.org/10.1016/j.jece.2021.105702.
[48] M.R. Saleh, H.M. El-Bery, H.N. Abdelhamid, Co@ZIF-8/TiO2 heterojunction for green hydrogen generation, Appl. Organomet. Chem. (2022), https://doi.org/10.1002/aoc.6995.
[49] H.N. Abdelhamid, Surfactant assisted synthesis of hierarchical porous metal-organic frameworks nanosheets, Nanotechnology 30 (2019) 435601, https://doi.org/10.1088/1361-6528/ab30f6.
[50] S. Saedy, N. Hiemstra, D. Benz, H. Van Bui, M. Nolan, J.R. van Ommen, Dual promotional effect of Cu_xO clusters grown with atomic layer deposition on TiO_2 for photocatalytic hydrogen production, Catal, Sci. Technol. 12 (2022) 4511–4523, https://doi.org/10.1039/D2CY00400C.
[51] L. Zhu, C.K. Nuo Peh, M. Gao, G.W. Ho, Hierarchical Heterostructure of TiO 2 Nanosheets on CuO nanowires for enhanced photocatalytic performance, Procedia Eng. 215 (2017) 180–187, https://doi.org/10.1016/j.proeng.2017.11.007.
[52] C. Castañeda, F. Tzompantzi, A. Rodríguez-Rodríguez, M. Sánchez-Dominguez, R. Gómez, Improved photocatalytic hydrogen production from methanol/water solution using CuO supported on fluorinated TiO_2, J. Chem. Technol. Biotechnol. 93 (2018) 1113–1120, https://doi.org/10.1002/jctb.5470.
[53] T.N. Ravishankar, M.O. de Vaz, S.R. Teixeira, The effects of surfactant in the sol–gel synthesis of CuO/TiO_2 nanocomposites on its photocatalytic activities under UV-visible and visible light illuminations, New J. Chem. 44 (2020) 1888–1904, https://doi.org/10.1039/C9NJ05246A.
[54] L. Yan, F. Yang, C. Tao, X. Luo, L. Zhang, Highly efficient and stable Cu_2O–TiO_2 intermediate photocatalytic water splitting, Ceram. Int. 46 (2020) 9455–9463, https://doi.org/10.1016/j.ceramint.2019.12.206.
[55] J. Yu, Y. Hai, M. Jaroniec, Photocatalytic hydrogen production over CuO-modified titania, J. Colloid Interface Sci. 357 (2011) 223–228, https://doi.org/10.1016/j.jcis.2011.01.101.
[56] Z. Zhu, C.-T. Kao, B.-H. Tang, W.-C. Chang, R.-J. Wu, Efficient hydrogen production by photocatalytic water-splitting using Pt-doped TiO_2 hollow spheres under visible light, Ceram. Int. 42 (2016) 6749–6754, https://doi.org/10.1016/j.ceramint.2016.01.047.
[57] R. Abe, K. Sayama, K. Domen, H. Arakawa, A new type of water splitting system composed of two different TiO_2 photocatalysts (anatase, rutile) and a IO_3^-/I^- shuttle redox mediator, Chem. Phys. Lett. 344 (2001) 339–344, https://doi.org/10.1016/S0009-2614(01)00790-4.
[58] A.M. Huerta-Flores, F. Ruiz-Zepeda, C. Eyovge, J.P. Winczewski, M. Vandichel, M. Gaberšček, N.D. Boscher, H.J.G.E. Gardeniers, L.M. Torres-Martínez, A. Susarrey-Arce, Enhanced photocatalytic hydrogen evolution from water splitting on ta 2 O 5 /SrZrO 3 Heterostructures decorated with cu x O/RuO 2 Cocatalysts, ACS Appl. Mater. Interfaces 14 (2022) 31767–31781, https://doi.org/10.1021/acsami.2c02520.
[59] J.A. Rodríguez, J. Evans, J. Graciani, J.-B. Park, P. Liu, J. Hrbek, J.F. Sanz, High water−gas shift activity in TiO2 (110) supported cu and au nanoparticles: role of the oxide and metal particle size, J. Phys. Chem. C 113 (2009) 7364–7370, https://doi.org/10.1021/jp900483u.
[60] H. Chen, Z.-G. Gu, S. Mirza, S.-H. Zhang, J. Zhang, Hollow cu–TiO2/C nanospheres derived from a Ti precursor encapsulated MOF coating for efficient photocatalytic hydrogen evolution, J. Mater. Chem. A 6 (2018) 7175–7181, https://doi.org/10.1039/C8TA01034J.
[61] Y. Wang, M. Zhou, Y. He, Z. Zhou, Z. Sun, In situ loading CuO quantum dots on TiO_2 nanosheets as cocatalyst for improved photocatalytic water splitting, J. Alloys Compd. 813 (2020) 152184, https://doi.org/10.1016/j.jallcom.2019.152184.
[62] Y. Yuan, K. Sheng, S. Zeng, X. Han, L. Sun, I. Lončarić, W. Zhan, D. Sun, Engineering cu/TiO2 @N-doped C interfaces derived from an atom-precise Heterometallic cu II 4 Ti IV 5 cluster for efficient photocatalytic hydrogen evolution, Inorg. Chem. 59 (2020) 5456–5462, https://doi.org/10.1021/acs.inorgchem.0c00084.
[63] V. Polliotto, S. Livraghi, A. Krukowska, M.V. Dozzi, A. Zaleska-Medynska, E. Selli, E. Giamello, Copper-Modified TiO_2 and $ZrTiO_4$: Cu Oxidation State Evolution during Photocatalytic Hydrogen Production, ACS Appl. Mater. Interfaces 10 (2018) 27745–27756, https://doi.org/10.1021/acsami.8b05528.
[64] M.Z. Hussain, Z. Yang, B. van der Linden, W.R. Heinz, M. Bahri, O. Ersen, Q. Jia, R. A. Fischer, Y. Zhu, Y. Xia, MOF-derived multi-heterostructured composites for enhanced photocatalytic hydrogen evolution: deciphering the roles of different components, Energy Fuel 36 (2022) 12212–12225, https://doi.org/10.1021/acs.energyfuels.2c02319.
[65] M.Z. Hussain, B. van der Linden, Z. Yang, Q. Jia, H. Chang, R.A. Fischer, F. Kapteijn, Y. Zhu, Y. Xia, Bimetal–organic framework derived multi-heterostructured TiO_2/Cu_xO/C nanocomposites with superior photocatalytic H_2 generation performance, J. Mater. Chem. A 9 (2021) 4103–4116, https://doi.org/10.1039/D0TA10853G.

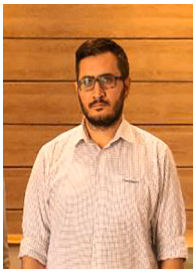

Hani Nasser Abdelhamid is Associate Professor at Al Imam University, Saudi Arabia. He obtained his M.Sc. in 2013 in Nanomedicine and Nanobiotechnology from National Sun Yat-Sen University (NSYSU, Republic of China, Taiwan), and Ph.D. in Inorganic Chemistry in 2017 at Stockholm University (Sweden). He is working in materials science, focusing on the synthesis, characterization, and applications of nanomaterials such as carbon-based nanoparticles (NPs), metallic NPs, metal oxide NPs, quantum dots (QDs), metal-organic frameworks (MOFs), covalent organic frameworks (COFs), polymer of intrinsic microporosity, nanocellulose, and chitosan. He applied these materials for biomedical, energy, and environmental-based applications. He published more than 177 articles in peer-reviewed journals, 40 book chapters, and filled 5 patents. According to Scopus and Google Scholar, he achieved an H-index of 65 and 71, respectively (May 2025). He received several international and national prizes including; The Creativity and Innovation Award in Green Economy and Renewable Energy, the Arab League Educational, Cultural, and Scientific Organisation (ALECSO, 2024) Award; the Obada International Prize for Young Distinguished Researchers (2023); Mohamed Farid Khamis Research Excellence Award winners; The British University in Egypt, Cairo, Egypt (2022); State Encouragement Awards of Egypt (2020); The best Research award, Assiut University, Assiut (2020); The Best 15 Inventions for Universities and Institutes, Connect Arabs, Egypt (2019); Scinopharm Award for Analytical Chemistry in graduate Thesis, Chinese Chemical Society (2013); The Phi-Tau-Phi Scholastic Honor Society of the Republic of China (2013). He was listed 7 Sucessive timesin "WORLD RANKING OF TOP 2% SCIENTISTS" according to the survey given by Stanford University; 2019-2024.